Analyzing the Responses of a Thermally Modulated Gas Sensor Using a Linear System Identification Technique for Gas Diagnosis

Faramarz Hossein-Babaei, *Member, IEEE*, and Seyed Mohsen Hosseini-Golgoo

Abstract—A novel approach to the problem of diagnostic data extraction from the responses of a thermally modulated resistive gas sensor (RGS) is presented. The RGS affected by a target gas (TG) is considered a black box dynamic system. The input to the system is the time-varying voltage applied to the heating element of the RGS, and the transient response of the RGS is the output. The structure of the defined system varies with the nature and concentration of the prevailing TG, and the parametric system identification techniques employed reveal system parameters differentiated only by the existing dissimilarities between the TGs. The discriminative information content of these parameters is, then, extracted by standard mathematical tools and utilized for TG recognition. Air contaminated with four different combustible vapors, methanol, ethanol, 2-propanol, and 1-butanol, each at 13 different contamination levels, was used to define 52 different systems. In each case, the transient response of the system to a staircase voltage waveform input was recorded. Computer modeling, based on *autoregressive moving average with exogenous input* (ARMAX) model, rendered different sets of system parameters which afforded feature extraction and TG classification by standard mapping tools. The method was verified by the successful classification of unknown TGs at undetermined contamination levels.

Index Terms—ARMAX model, artificial olfaction, feature extraction, linear system identification, resistive gas sensor, thermal modulation.

I. INTRODUCTION

RESISTIVE GAS SENSORS (RGS) [1]–[6] are cost effective, small, easy to use, and durable, and their applications range from the simplest household CO and fire detectors [1]–[4], [7] to sensor arrays utilized in sophisticated industrial electronic noses [8]–[11]. The response of these devices to any polluting, combustible, or poisonous target gas (TG) occurs as a shift in the electrical resistance of the sensor [2]–[5] and, therefore, no selective detection or gas diagnosis is expected from a single RGS. RGSs are made of polycrystalline oxide semiconductors. In a detection process, reducing TG species interact with the oxygen atoms present at the effective surface of the oxide solid and cause a temporal change of conductivity which is transformed into a measurable electrical quantity and recorded as the response of the sensor. The complicated gas-solid interaction taking place at the surface of the oxide semiconductor is strongly temperature dependent; and the nature of this dependence varies from one TG to the next. Although this gas-solid interaction process has been the subject of numerous research works [12]–[15], the complexity of the reaction and the scarcity of the quantitative data hinder quantitative predictions on such reactions.

Different techniques have been used to overcome the lack of selectivity in these sensors [8], [16]–[21], among which is the analysis of the dynamic responses of a thermally modulated RGS [21]–[28]. RGSs operate at elevated temperatures, and their temporal response to a TG is strongly dependent on the operating temperature. A preprogramed variation of the operating temperature results in a complex temporal response that contains information on the nature and concentration of the TG [22]. It has been shown that the extraction of this information from the temporal response patterns corresponding to an unknown TG may afford gas diagnosis [23]–[27].

Different types of power waveforms have been applied to the heating element of the RGS to provide a variety of time varying operating temperatures [23]–[28]. An example of this kind is a staircase voltage applied to the sensor heater [25]. Due to the small thermal capacity of the sensor and its heating device, each step of the staircase can quickly provide the corresponding temperature plateau and allow enough time for the sensor response to approach its respective steady-state level. This temperature modulation created different temporal response patterns containing discriminatory information. The recorded response patterns have been processed, either in time [25] or frequency [26] domains, for the extraction of their diagnostic information content.

System identification techniques have been utilized to model the response of RGS to a known TG [29]. In a chemical sensor, the analyte is labeled as the input to the system, and the steady-state response of the sensor as the output [30]–[32]. In this way, the sensing system is mathematically identified based on the experimentally obtained dynamic data. The analysis has been carried out by the utilization of either parametric [30] or nonparametric [31], [32] methods. Although the process of chemical detection is nonlinear, researchers have attempted identification of the defined systems based on linear models [31]–[35]. *Autoregressive with exogenous input* (ARX) model has successfully been employed for the modeling of a fire detector [33]. In this case, the loss of mass of the burning material was defined as the input of the system, and the sensor response was con-

sidered the output. In diagnostic chemical sensors, however, an unknown input (the analyte) further complicates the analysis of the sensing system. This problem has been dealt with by "inverse modeling" [36]. The method was employed for the linear black-box modeling of gas sensor arrays [30]–[32], [34].

Pardo *et al.* analyzed the responses of a four-component sensor array using both linear and nonlinear models [30]. For gas diagnosis, however, they utilized two different nonlinear inverse models which could determine the composition of a toluene-octane gas mixture [31], [32]. Searle *et al.* treated the transient responses of the elements of a six-component sensor array as the inputs to the defined inverse system, while the unknown odor was considered the output [34]. They utilized linear modeling, and successfully used the system for bacteria classification [34]. Kunt *et al.* used a nonlinear system analysis technique for the extraction of the discriminative information from the responses of a RGS temperature modulated by an optimized voltage pulse train, and showed that the amount of the extractable discriminative information varies with the configuration of the temperature modulating waveform [27]. The emphasis of the above referenced investigations, as well as the present work, is on TG classification rather than the determination of its concentration. The TG concentration can be determined based on the steady-state response of a general sensor and the related calibration data, subsequent to a successful classification [34].

This work introduces a novel approach to the problem of discriminative feature extraction from the responses of a temperature modulated RGS by defining the TG affected sensor as a single-input–single-output (SISO) dynamic system. By this definition, the contaminated atmosphere surrounding the sensor becomes a part of the black box, and the defined system varies structurally when encountered with different TGs. The staircase voltage applied to the microheater of the sensor is considered the input to the system, and the temporal response of the sensor is the output. This approach allows the utilization of appropriate linear black-box modeling tools for the numerical description of these features which are, subsequently, classified by classic classification techniques [37], [38]. The procedure was applied to the experimental data related to four different TGs each at 13 different concentrations. Although the TGs examined were of obvious chemical similarities, the method afforded their discrimination in the verification experiments.

II. THEORY

The system analyzed is schematically depicted in Fig. 1. It comprises a RGS heated with a low thermal capacity resistive heating element, a few well defined circuit components, and the gaseous atmosphere of the box. The latter component of the system consists of air polluted with a known concentration of a TG. All of the physical and chemical parameters of this atmosphere are assumed to be time-invariant; i.e., the volume of the box is assumed to be large enough to accommodate the minor compositional alterations occurring due to the gas-solid interactions at the effective surface of the RGS.

As depicted in Fig. 1, the time varying voltage applied to the microheater $u(t)$ is the input to the system. The output of
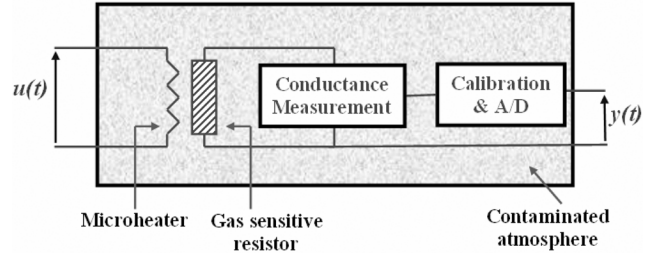

Fig. 1. The schematic diagram of the system analyzed. The atmosphere within the box is a significant component of the system.

the system is a time-dependent numerical function $y(t)$ proportional to the varying conductance of the RGS. The defined system is of the SISO type. Although the structure of the system appears simple, it is complicated due to the cumbersome time- and temperature-dependent electronic interactions between the gaseous species and the effective surface of the RGS. These interactions alter the electronic properties of the sensor element with time, and hence, the defined system is dynamic. The input voltage changes the temperature at the surface of the RGS which, in turn, alters both the nature and the intensity of these interactions. The output of the system is, according to Fig. 1, determined by the electrical conductance of the RGS which is strongly affected by both the surface temperature and the interactions with the gaseous species present. The present knowledge on the nature and kinetics of these gas-solid interactions is qualitative and cannot facilitate quantitative predictions regarding the output. The lack of quantitative information on the intricate time and temperature dependent processes taking place inside the system makes the defined system a black box.

The gas-solid interactions occurring within the system are nonlinear [13]–[15], [31] but here, linear models are examined for the first approximate analysis of the black box defined. This analysis results in a parametric categorization of the system's responses by way of "system simulation" rather than "response prediction" [40]. The justification of the linear approximation assumed is presented in Section IV, where the close fitting of the computer modeling results to the experimental data is demonstrated.

A linear dynamic SISO system, in general, is described by the following model [40], [41]:

$$A(q)y(t) = \frac{B(q)}{F(q)}u(t - n_k) + \frac{C(q)}{D(q)}e(t) \qquad (1)$$

in which $e(t)$ is a white noise of zero-mean value, n_k is the "input delay," and $A(q), B(q), C(q), D(q)$ and $F(q)$ are as defined below

$$\begin{aligned}
A(q) &= 1 + a_1 q^{-1} + a_2 q^{-2} + \ldots + a_{na} q^{-na} \\
B(q) &= b_1 + b_2 q^{-1} + \ldots + b_{nb} q^{-nb+1} \\
C(q) &= 1 + c_1 q^{-1} + c_2 q^{-2} + \ldots + c_{nc} q^{-nc} \\
D(q) &= 1 + d_1 q^{-1} + d_2 q^{-2} + \ldots + d_{nd} q^{-nd} \\
F(q) &= 1 + f_1 q^{-1} + f_2 q^{-2} + \ldots + f_{nf} q^{-nf} \qquad (2)
\end{aligned}$$

where q^{-n} is the backward shift operator, i.e., $q^{-1}x(t) = x(t - 1), q^{-2}x(t) = x(t - 2), \ldots$ and a_i, b_i, c_i, d_i and f_i are the unknown parameters of the system, and n_a, n_b, n_c, n_d and n_f are

their respective orders. (In simple terms, $A(q) \cdot y(t)$, for instance, is a parametric sum of the y values at time t and before; and n determines the length of the y's history considered.) The parameter vector is defined as

$$\theta = (a_1 a_2 \ldots a_{na} b_1 b_2 \ldots b_{nb} f_1 f_2 \ldots f_{nf} \ldots$$
$$c_1 c_2 \ldots c_{nc} d_1 d_2 \ldots d_{nd})^T. \quad (3)$$

The determination of the parameter vector components facilitates a mathematical relationship between the input and the output of the system.

Simplified special cases of this general model, such as Box–Jenkins [42] and *autoregressive moving average with exogenous input* (ARMAX) [43] models, have successfully been utilized for the modeling of engineering, industrial, and economical systems of different natures [44]. After a number of trials on the different versions of the general model, ARMAX, obtained for $n_f = n_d = 0$, was utilized for the modeling of the sensory system studied. This structure, along with its orders is presented as $\text{ARMAX}(n_a, n_b, n_c, n_k)$. The criteria in the model selection were the simplicity of the model and its ability to closely simulate the experimentally recorded system outputs. In this model, the input and the output of the system are related through the following relationship:

$$A(q)y(t) = B(q)u(t - n_k) + C(q)e(t) \quad (4)$$

where the operators A, B, and C are defined according to (2) by the following parameter vector:

$$\theta = (a_1 a_2 \cdots a_{na} b_1 b_2 \cdots b_{nb} c_1 c_2 \cdots c_{nc})^T. \quad (5)$$

The method used for the estimation of θ was "prediction error-based" [41], and the calculations of the components were carried out based on the comparisons between the simulated outputs and the experimentally recorded data. The main steps of the process are briefly given in the Appendix.

In simple words, the components of the θ vector and the orders were determined based on the selection of the combinations which could result in simulated system outputs best fitting to the experimental data. The estimated θ, for each system (each different atmospheric composition in the test chamber) was assumed as the high-dimensional feature vector of the prevailing atmosphere. The classification of the TGs (see Section IV) was, then, achieved by mapping of these vectors to a space of lower dimensions.

III. EXPERIMENTAL

The experimental layout is schematically presented in Fig. 2. A 20-liter soda-lime glass container was used as the controlled atmosphere chamber. The target gases used were methanol, ethanol, 2-propanol, and 1-butanol vapors. Predetermined volumes of the liquid alcohols were injected onto a miniature borosilicate glass dish inside the chamber and heated mildly (to ~ 60 °C) with a hermetically covered voltage controlled electrical heater to assist alcohol evaporation. The total evaporation of the contaminant created different contamination
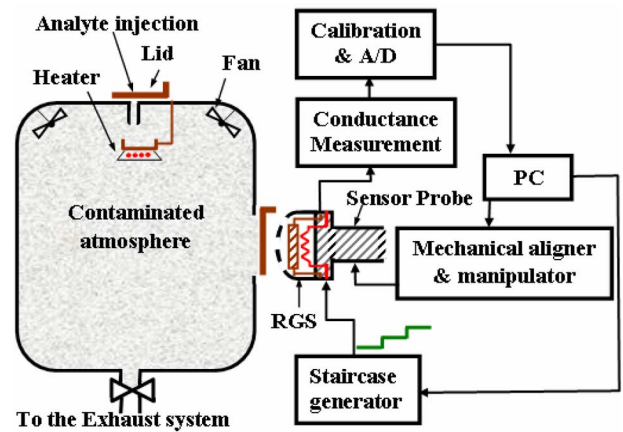

Fig. 2. Schematics of the experimental setup.

levels, in the range of 250–3000 w-ppm, in the closed chamber. Prior to each experiment, the chamber atmosphere was mildly agitated for homogenization by two small electric fans placed inside the chamber. The contamination levels were continuously monitored before and during the measurements by a calibrated reference gas sensor placed inside the chamber. This monitoring of the contamination level was to confirm the maintenance of a constant concentration of the contaminant during the measurements. The chamber could maintain a constant TG concentration for 5 h before dropping 5% below its original level. The actual TG concentration level is naturally represented in the shape of the transient response profile, and, therefore, inevitably and significantly present in the entire mathematical process of gas diagnosis. The nominal concentrations, obtained by dividing the mass of the evaporated alcohol to the mass of the chamber air, were used for the labeling of the training and verification data recorded. The concentration data are provided to facilitate the possibility of comparison with the prior and future investigations. The ambient temperature and the relative humidity in the laboratory were continuously monitored during the experiments; the respective variations throughout the experiments were 23 °C–28 °C and 30%–45%.

The RGS employed was a commercially available general gas detector (SP3-AQ2, FIS Company, Japan). The device consists of a tin oxide thick-film sensing element of ~ 2.3 mm^2 active area, and a microheater to provide the elevated working temperatures required for its operation. Further information on this sensor can be obtained from the website of the company [45]. The sensor utilized is of low cost (~ 7 USD), and its availability in the international market facilitates the reproduction of similar experimental database (see below) and the extension of the work in different orientations by interested researchers.

The operating temperature of the RGS changes by altering the voltage applied to the microheater. A constant voltage level corresponds to a constant working temperature at the sensitive surface of the RGS, while a varying voltage waveform results in a time-varying operating temperature. The resistance of the RGS depends on both the temperature maintained at the sensitive surface of the device and the composition of the surrounding atmosphere. The relationship between the conductance and the surface temperature of the RGS used was determined by the
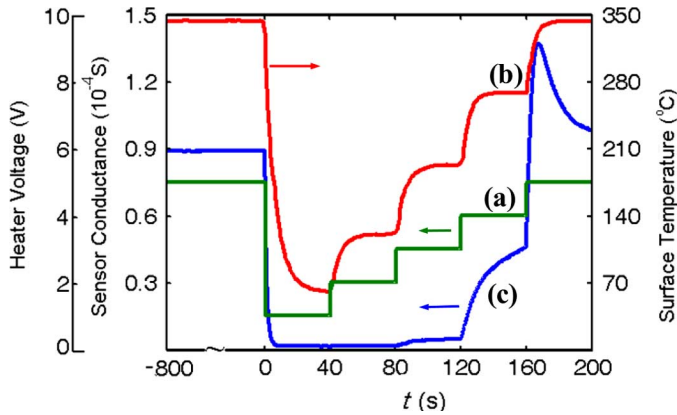
Fig. 3. The temporal variations of: (a) the voltage applied to the microheater of the sensor; (b) the surface temperature; and (c) the electrical conductance of the sensor, both measured in clean air.

measurement of the device resistance at different operating temperatures in clean air. The surface temperature was varied by the variation of the applied microheater voltage, and was measured by placing a fine (diameter of 0.04 mm) platinum-based thermocouple junction in the physical contact with the sensitive surface of the sensor. For these measurements, the porous cap of the sensor had to be removed. The relationship between the applied heater voltage, surface temperature of the tin oxide pallet, and the conductance of the device measured in clean air is presented in Fig. 3.

The chamber has a gas impermeable lid which opens to allow the insertion of the RGS probe, schematically depicted in Fig. 2, into the chamber. The time-varying voltage applied to the microheater, to modulate the operating temperature of the RGS, is a staircase voltage waveform. As shown in Fig. 3(a), this waveform consists of five different voltage steps, from 1 to 5 V, with a 40 s wide plateau at each step. Prior to each experiment, the device was preheated by applying a continuous 5 V (the nominal heating voltage of the RGS employed) for a period of 10 min in clean air. This preheating was to clean up the surface of the gas sensitive oxide from the residues of the previous measurements, bring it to a well established thermal equilibrium, and to stabilize the sensor at its steady-state condition in clean air.

The probe was, then, inserted into the chamber containing air contaminated with a predetermined concentration of a known TG. The heating voltage was kept at 5.0 V for another 3 min. During this period, the sensor remained at its steady-state response level in the contaminated atmosphere of the chamber. Starting at $t = 0$, the staircase waveform was applied to the sensor heater. It started with a step fall from 5 to 1 V, and, then, varied with time according to the steps depicted in Fig. 3(a), which, finally, brought the heating voltage back to the 5 V level at $t = 200$ s. This was carried out automatically by utilization of a computer programmable "multifunction card" (Advantech Company, USA; model-PCI-1711L). The probe was then extracted from the chamber and preheated for the next run. The output of the system was continuously recorded in $t = 0$–200 s range. Results obtained for methanol, ethanol, 2-propanol, and 1-butanol, each at 13 different concentration levels are given in Fig. 4(a)–(d), respectively.

IV. SYSTEM ANALYSIS

The recorded responses were digitized with a sampling rate of $100 \ \text{s}^{-1}$, and noise reduction was achieved by utilization of a moving average digital filter with a window length of 25 samples. The result is a database which contains 52 sets of data corresponding to the 52 temporal responses plotted in Fig. 4(a)–(d). The task is, then, to analyze the system and determine the system parameters respective to different conditions.

The recorded outputs in the broad time span of 0–200 s contain huge amounts of information which makes the system analysis cumbersome. Moreover, the mathematical analysis of this amount of information consumes so much of the computer time that makes the online operation of the gas diagnosis system impractical. To simplify the task, and based on the visible discriminative features of the recorded responses, the data were truncated to cover a selected time span of 120–200 s.

The presentation of the responses related to a five-step voltage staircase covering $t = 0$–200 s, as given in Fig. 4, and using only the response data related to two particular steps of the staircase may appear ambiguous. The following comments are made for clarification: (a) The response of a metal oxide RGS to any atmospheric condition depends on the history of the device [2], i.e., none of the segments of the response traces presented in Fig. 4 can be regenerated without repeating the background thermal and chemical history. (b) Voltage staircases have been used by other researchers [25] for diagnosis of other TGs by different mathematical approaches; the utilization of the staircase waveform was intended to facilitate a comparison of the outcomes from the different mathematical approaches. (c) Starting from a single step, the diagnostic information extracted proved insufficient for a successful classification of the four TGs examined. (d) For a two-step analysis, the apparent detailed features, the high amplitudes, and hence, the low recording noise levels involved made the combination of the steps IV and V attractive. The results of this analysis are presented below, which indicate the existence of discriminating information enough to classify the four TGs investigated. (e) More sophisticated analysis based on the information extraction from three or more steps is recommended for future attention in Section VI.

In both step IV and step V time intervals, $\text{ARMAX}(n, n, n, 1)$ was found to afford reasonable prediction error levels in the simulation of the response data. This model structure was selected for the modeling of the system. For the determination of the orders (values of n), the "fitness" levels (see the Appendix) of the models of different orders, averaged within the whole respective step range and over all the training runs related to each TG were compared. The results related to steps IV and V are presented in Fig. 5(a) and (b), respectively. Acceptable fitness throughout the data sets examined, occurred for $n = 1$ at step IV, and $n = 2$ at step V. The fitness values calculated for all of the experimental runs are presented in Table I, which indicate a fine compatibility between the experimentally recorded and simulated responses. The simulation results are compared with the experimentally recorded responses in Fig. 6(a)–(d). The close fitting of the simulated and the actual responses validates the linear approximation declared in Section II.

Based on the ARMAX(1, 1, 1, 1) and ARMAX(2, 2, 2, 1) model structures, the simulated outputs and the corresponding
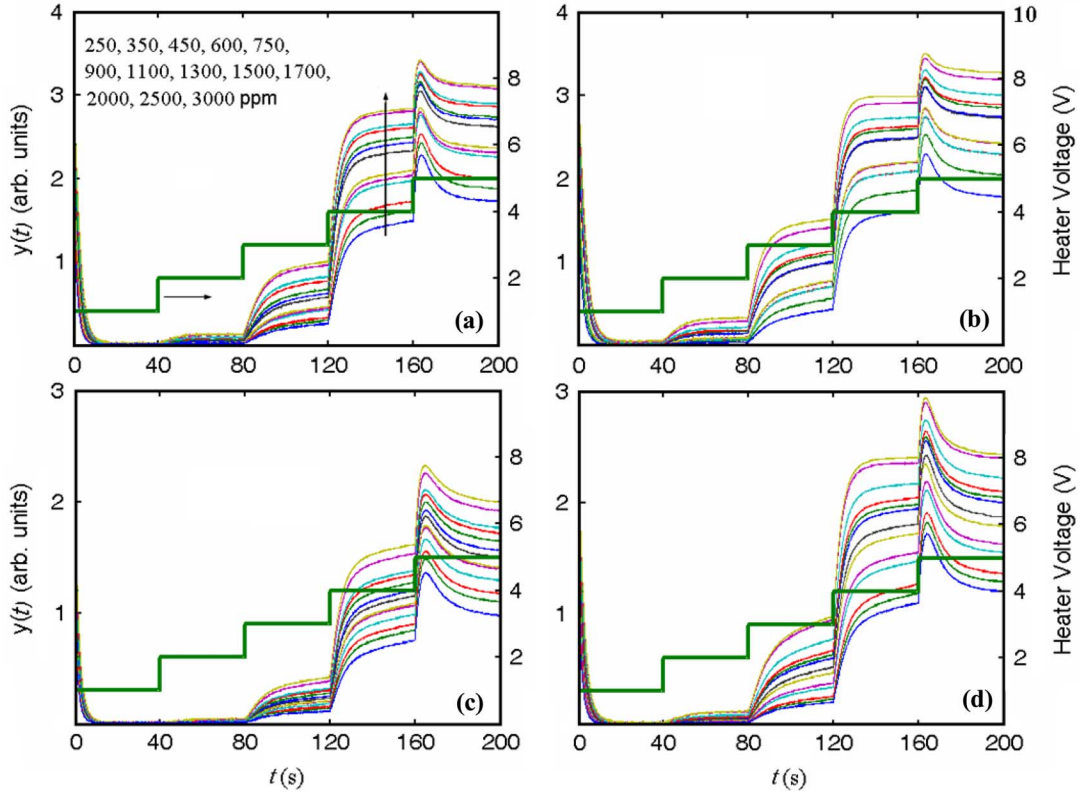
Fig. 4. The transient responses of the thermally modulated resistive gas sensor to various concentration levels of: (a) methanol; (b) ethanol; (c) 2-propanol; and (d) 1-butanol in air. The staircase heater voltage used for thermal modulation of the sensor is also presented in the diagrams.
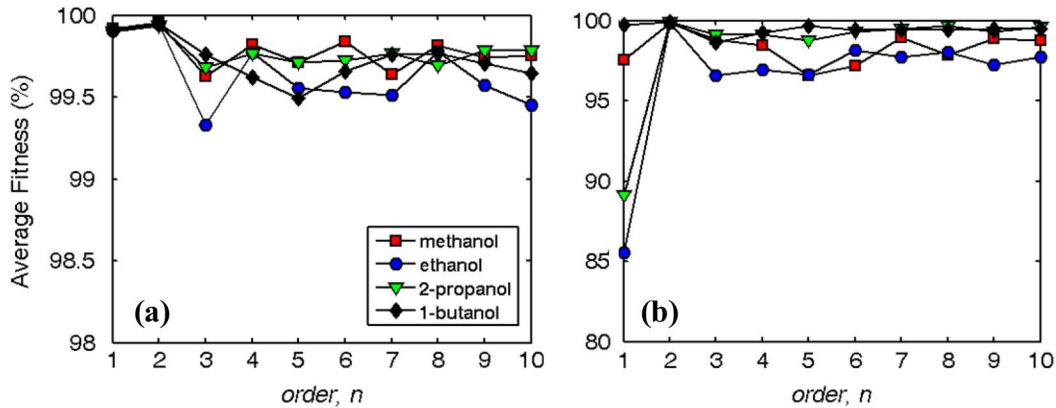

Fig. 5. The average "fitness" of the $\mathrm{ARMAX}(n, n, n, 1)$ models to the training data related to (a) step IV and (b) step V.

θ vectors related to steps IV and V acquire the following general forms, respectively:

$$y_{IV}(t) = \frac{b_1 q^{-1}}{1 + a_1 q^{-1}} u_{IV}(t) + \frac{1 + c_1 q^{-1}}{1 + a_1 q^{-1}} e(t)$$

$$\theta_{IV} = (a_1 b_1 c_1)^T \tag{6}$$

$$y_V(t) = \frac{b'_1 q^{-1} + b'_2 q^{-2}}{1 + a'_1 q^{-1} + a'_2 q^{-2}} u_V(t)$$

$$+ \frac{1 + c'_1 q^{-1} + c'_2 q^{-2}}{1 + a'_1 q^{-1} + a'_2 q^{-2}} e(t)$$

$$\theta_V = (a'_1 a'_2 b'_1 b'_2 c'_1 c'_2)^T \tag{7}$$

in which the subscripts IV and V refer to steps IV and V of the recorded responses, respectively. Hence, the total parameter vector is resulted as

$$\theta = \begin{pmatrix} \theta_{IV} \\ \theta_V \end{pmatrix} = (a_1 b_1 c_1 a'_1 a'_2 b'_1 b'_2 c'_1 c'_2)^T \tag{8}$$

in which the first three components are related to θ_{IV} and the rest are those of θ_V.

The components of the θ_{IV} and θ_V vectors corresponding to different experiments were calculated as described in the Appendix. The resulted parameter vectors are nine-dimensional, which are taken as the feature vectors of the different atmospheres present in the chamber. Considering the number

TABLE I
THE VALUES OBTAINED FOR THE "FITNESS" OF THE ARMAX(1, 1, 1,1) AND ARMAX(2, 2, 2,1) MODELS
TO THE TRAINING DATA RELATED TO STEPS IV AND V, RESPECTIVELY

| C (ppm)	Contaminant							
	Methanol		Ethanol		Propanol		Butanol	
	IV	V	IV	V	IV	V	IV	V
250	99.90	99.89	99.91	99.89	99.88	99.88	99.90	99.90
350	99.91	99.89	99.90	99.87	99.88	99.89	99.90	99.90
450	99.91	99.88	99.90	99.86	99.89	99.88	99.91	99.90
600	99.91	99.87	99.90	99.85	99.89	99.87	99.91	99.90
750	99.91	99.87	99.90	99.86	99.89	99.88	99.91	99.90
900	99.91	99.87	99.90	99.86	99.90	99.88	99.91	99.87
1100	99.91	99.85	99.90	99.84	99.90	99.88	99.91	99.90
1300	99.92	99.85	99.90	99.84	99.90	99.88	99.91	99.89
1500	99.92	99.85	99.90	99.83	99.90	99.87	99.91	99.89
1700	99.92	99.84	99.90	99.83	99.91	99.87	99.91	99.89
2000	99.92	99.84	99.90	99.82	99.91	99.87	99.91	99.89
2500	99.92	99.84	99.91	99.81	99.91	99.87	99.91	99.89
3000	99.92	99.84	99.91	99.80	99.91	99.87	99.91	99.89
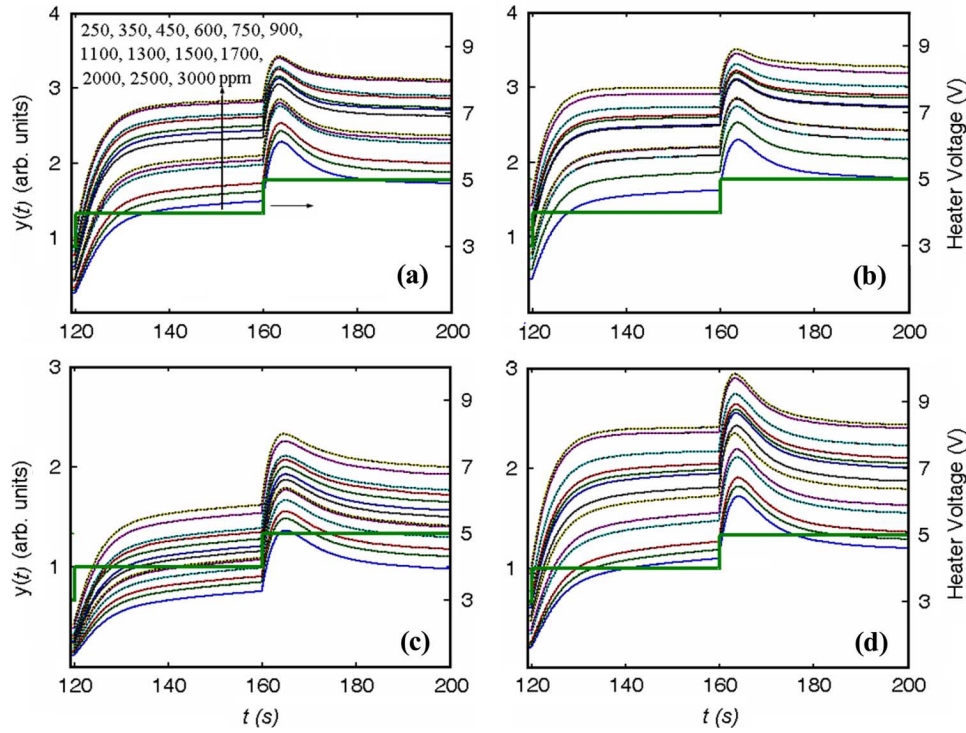
Fig. 6. The inputs and the outputs of the system at the presence of: (a) methanol; (b) ethanol; (c) 2-propanol; and (d) 1-butanol after filtering and data truncation (solid lines); the black dotted lines are the simulation results based on the mathematical model introduced.

of the different atmospheres investigated, 52 such vectors were generated. These vectors were employed for the construction of the following feature matrix:

$$X = \left(\theta_{\zeta 1}^m\, \theta_{\zeta 2}^m \cdots \theta_{\zeta 13}^m \theta_{\zeta 1}^e \theta_{\zeta 2}^e \cdots \theta_{\zeta 13}^e \right.$$
$$\left. \theta_{\zeta 1}^p \theta_{\zeta 2}^p \cdots \theta_{\zeta 13}^p \theta_{\zeta 1}^b \theta_{\zeta 2}^b \cdots \theta_{\zeta 13}^b \right). \quad (9)$$

The superscripts m, e, p and b stand for methanol, ethanol, 2-propanol, and 1-butanol, respectively, while the subscripts $\zeta_1, \zeta_2, \ldots$ and ζ_{13}, are to indicate the 13 different TG concen-

tration levels given in Table I. Replacing (8) in (9) results in the final form of the feature matrix

$$X = \begin{pmatrix} (a_1)_{\zeta 1}^m & \cdots & (a_1)_{\zeta 13}^m & (a_1)_{\zeta 1}^e & \cdots & (a_1)_{\zeta 13}^e \\ \vdots & \ddots & \vdots & \vdots & \ddots & \vdots \\ (c_2')_{\zeta 1}^m & \cdots & (c_2')_{\zeta 13}^m & (c_2')_{\zeta 1}^e & \cdots & (c_2')_{\zeta 13}^e \\ (a_1)_{\zeta 1}^p & \cdots & (a_1)_{\zeta 13}^p & (a_1)_{\zeta 1}^b & \cdots & (a_1)_{\zeta 13}^b \\ \vdots & \ddots & \vdots & \vdots & \ddots & \vdots \\ (c_2')_{\zeta 1}^p & \cdots & (c_2')_{\zeta 13}^p & (c_2')_{\zeta 1}^b & \cdots & (c_2')_{\zeta 13}^b \end{pmatrix}_{9 \times 52}. \quad (10)$$
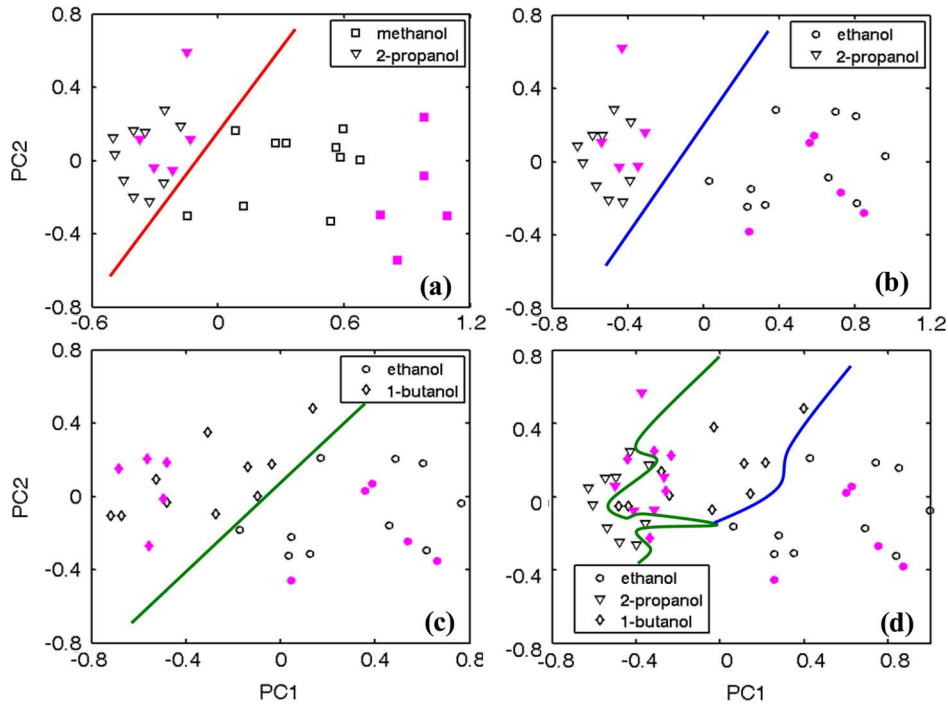
Fig. 7. The results of applying the PCA mapping to the training (unfilled markers) and verification (filled markers) databases of different (a)–(c) 2-gas and (d) 3-gas systems to a two-dimensional feature space for target gas classification.

Hence, each differently contaminated chamber atmosphere is described by a combination of nine figures, say components of a nine-dimensional feature vector, which form a column in the above described feature matrix. The number of the columns in this matrix is equal to the number of the responses recorded which are related to four different classes of m, e, p, and b. In Section V, the task is to use different mathematical tools for classification of the recorded responses based on their respective feature vectors. The combination of the mathematical transformations leading to a successful classification can then be applied on the feature vector of an unknown contamination to determine its class.

V. TARGET GAS CLASSIFICATION

System classification based on a high-dimensional θ vector is difficult, and it is favorable to map the data from the θ-space to a space of 1, 2, or 3 dimensions, which affords graphical visualization. This mapping is to preserve and clarify as much of the discriminating features of the θ vectors as possible. Among the mapping techniques used for feature extraction from high-dimensional feature matrices, Principal Component Analysis (PCA) [37], [38] and Linear Discriminant Analysis (LDA) [38], [39] are the most common; and both were examined as the mapping tools in the present classification problem. The interested reader may obtain comprehensive information on these classification techniques in the above given references. The results follow.

Using PCA, the feature vectors were mapped onto a two-dimensional feature space. Ten feature vectors of each class, all in the concentration range of 350–2000 ppm, were considered for PCA training. The work failed to render a successful classification of the four classes. However, applied to feature matrices

constructed of the feature vectors related to two TGs, the method demonstrated neat delineation of the classes. Subsequently, the same mapping tool was applied to the verification data which comprised a total of 20 output recordings (five of each TG). The verification recordings were carried out, in conditions similar to the acquisition of the training data 15 days after the completion of the training work. The results are given in Fig. 7(a)–(c), which indicate the successful classification of the verification data. In Fig. 7(b), for instance, PCA has successfully differentiated both the training (unfilled markers) and verification (solid markers) vectors related to methanol and 2-propanol from each other with zero failure rates. However, in a three-class categorization test, while PCA successfully segregated the training data into three separate classes, as shown in Fig. 7(d), it failed to segregate the verification data related to p and b classes. This verification data percolation is depicted in Fig. 7(d).

In a second attempt, LDA was applied to the feature matrix given in (10) for the purpose of classification. Thirteen feature vectors of each class, all in the concentration range of 250–3000 ppm, were considered for LDA training. Based on a number of trial mappings, 2 out of these 52 parameter vectors, both related to the e class, were found to be of insufficient accuracy and were discarded from the training matrix. The result of the LDA mapping of the 50 training parameter vectors of the 4-gas system to a three-dimensional feature space is presented in Fig. 8(a) with unfilled markers. Fig. 8(a) depicts a distinct class segregation of the training vectors, which is also observable in the F_1-F_2 and F_1-F_3 two-dimensional projections shown in Fig. 8(b) and (c). The same mapping operator was then applied to all of the 20 verification parameter vectors introduced in the previous paragraph. The results, given in Fig. 8(a)–(c) with pink filled markers, indicate the allocation of all the 20 verification tests into their appropriate class volumes.
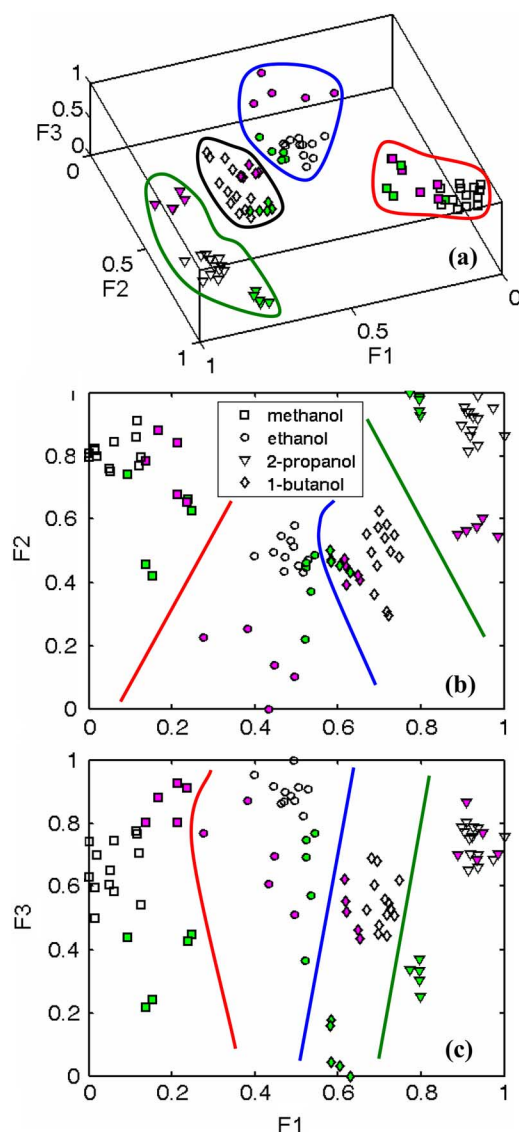
Fig. 8. The results of the LDA mapping of the training (unfilled markers), the first verification (pink filled markers) and the second verification (green filled markers) databases to an (a) three-dimensional and (b) and (c) two-dimensional feature spaces for the classification of the target gases in a 4-gas system.

The effectiveness of the latter classification technique was examined once more by its application on a second set of verification data recorded 45 days after the preliminary training data recording. The intention was to observe the negative effects of the sensor's drift, due to aging, irreversible environmental poisoning, or change of experimental conditions such as humidity and temperature in the laboratory, in the results of the gas classification procedure presented. The total number of the experiments was 20, 5 of each TGs investigated, and the target gas concentration levels were in 500–1700 ppm range. The results are presented in Fig. 8(a)–(c) using green filled markers. Despite the fact that the positions of these responses in the feature space are significantly shifted with respect to the training feature vectors, they have all been allocated to their correct classes.

VI. DISCUSSION

By selecting four TGs with obvious chemical similarities, the intention was to examine the inherent diagnostic and discriminative information content of the transient responses of an RGS enriched by temperature modulation. The definition of the sensory system as a black box of well defined and easy to measure input and output facilitated the application of the powerful system analysis techniques to extract the diagnostic information related to the analyte which is, by definition, a significant part of the system. The system went through identical preheating periods prior to each recording to assure similar sensor histories throughout the experiments. This proved to be a key technical point in the proper clustering of the feature vectors in the feature space. The elimination of these preheating cycles caused feature vectors of the same TG to scatter and hindered effective classification.

The voltage waveform utilized as an input to the system covered approximately the full operating temperature range of the tin oxide-based RGS, which is limited to ~100 °C–350 °C. The limitations are due to low sensitivity and humidity caused errors below 100 °C and irreversible transitions and rapid aging above 350 °C. However, there is still room to optimize this voltage waveform as the duration and number of the voltage plateaus can be adjusted for the fortification of the system output with the diagnostic information. Moreover, in this work, only two out of the five recorded response steps were analyzed and the rest of the output left unattended. Although the selected steps apparently contained the most detailed features, the extraction of the useful information from other steps of the output would have advanced the identification process and initiated further TG discriminating power. With all these enhancement possibilities intact, the method successfully categorized the four TGs introduced.

In a practical odor diagnosis, e.g., in the classic case of coffee categorization [46], or in an odor-based detection of the microorganisms [34], the concentration of the analyte is not precisely controlled, but the TG can be restricted to remain in a predetermined concentration range by the utilization of a reference RGS and dilution of the analyte with clean air if necessary. In the present work, the broad analyte concentration range of 250–3000 ppm was investigated to form the training database, but the verification tests were carried out in the 500–1700 ppm concentration range which allows a droplet of the unknown precursor liquid to be introduced into the chamber for evaporation using a medium accuracy sampler.

The sensor drift, whether caused by its natural aging or occurred temporarily by the variation of the atmospheric parameters, such as relative humidity, can interfere with the gas identification process. Although the system was able to classify the unknown TGs introduced 45 days after the training process, the respective vectors produced in the feature space (see Fig. 8) drifted substantially far from the training points. Similar problems are common among the artificial olfaction systems, and even elaborate electronic noses suffer from the drift of their sensor arrays which require frequent recalibration or replacement. The problem is less detrimental in the gas diagnosis system described as it contains only one chemical sensor; and the drift monitoring and calibration are much easier in single sensors than arrays. Replacing one sensor with another of the same type, however, required a repeat training process to form a new database. This is understood based on the inevitable structural differences between the electroceramic pallets and, particularly, the microheaters of the sensors.

VII. CONCLUSION

A systematic procedure for the extraction of the discriminative information from the responses of a thermally modulated resistive gas sensor was introduced. The procedure consisted of three independent blocks: Definition of the system with explicit and easy to measure input and output and the accumulation of an appropriate input/output database; the analysis of the database for system identification; and the extraction of the discriminating information from the system parameters utilizing standard pattern recognition tools. By defining the RGS, together with its contaminated surrounding, as a dynamic system, the time-varying voltage applied to the microheater of the sensor could be considered the input. As a result, the complications involved with the analysis of a system with unknown chemical input were removed, and a linear parametric system identification technique could be employed to analyze the responses recorded. The procedure was enabled to classify methanol, ethanol, 2-propanol, and 1-butanol vapors, in a wide concentration range in air, by the utilization of the ARMAX model structure for the linear black box modeling of the systems containing different atmospheric compositions and the LDA for the classification of their parameter vectors in a three-dimenssional feature space.

The four contaminants examined bore considerable chemical similarities, and their segregation in the feature space is a clear indication of the vast inherent potentials of the thermally modulated RGS in the field of gas diagnosis. It also demonstrates the presence of an incredible amount of diagnostic information in the transient responses of the gas sensors in general, and justifies further efforts to enhance the art of enrichment and extraction of this information.

APPENDIX

The general model, given in (1), can be rewritten as [40]

$$y(t) = G(q;\theta)u(t - n_k) + H(q;\theta)e(t) \tag{1a}$$

in which

$$G(q;\theta) = \frac{B(q)}{A(q)F(q)} \text{ and } H(q;\theta) = \frac{C(q)}{A(q)D(q)}. \tag{2a}$$

The parameter vector, defined by (3), is estimated by the utilization of "prediction error method" [41]. It has been shown that the optimal predictor of the model given in (1a) has the following form [41]:

$$\hat{y}(t|\theta) = H^{-1}(q;\theta)G(q;\theta)u(t - n_k)$$
$$+ (1 - H^{-1}(q;\theta))y(t) \tag{3a}$$

in which the superscript ^ is to distinguish the estimated results from the actual values. For $H(q;\theta) = 1$, the optimal predictor will assume the following form:

$$\hat{y}(t|\theta) = G(q;\theta)u(t - n_k). \tag{4a}$$

The G-related parameters of the system [a_i, b_i, and f_i, as given in (3)] are calculated based on (4a) through the following procedure.

For each combination of the parameters the "prediction error" is calculated according to

$$\varepsilon(t,\theta) = y(t) - \hat{y}(t|\theta). \tag{5a}$$

The parameters are, then, selected based on the minimization of the following "loss function" [41]:

$$V_N(\theta) = \frac{1}{N} \sum_{t=1}^{N} \varepsilon^2(t,\theta) \tag{6a}$$

in which N is the number of the samples determining an experimentally recorded y(t). Different interactive numerical search routines, such as Gauss–Newton and Levenberg–Marquardt [47] can be utilized for the calculation of the local minima of (6a). In this work the appropriate search routine was automatically selected by the software employed.

For estimation of the H-related parameters of the system [c_i and d_i, as given in (3)], $G(q;\theta)$ is kept fixed at its previously estimated values and the optimal predictor, given in (3a), is utilized for a second time. In this case, (3a) assumes the following configuration:

$$\hat{y}(t|\theta) = H^{-1}(q;\theta)\hat{G}(q;\theta)u(t - n_k)$$
$$+ (1 - H^{-1}(q;\theta))y(t). \tag{7a}$$

Similar to the previous case, the estimation of the H-related parameters is afforded by searching for the local minima of (6a) [48].

After the estimation of all the components of the $\hat{\theta}$-vector ($\hat{\theta}$ is replaced by θ in the main text), an assessment of the model is afforded by the prediction of the output of the system; using the following predictor:

$$\hat{y}(t|\hat{\theta}) = \hat{H}^{-1}(q;\theta)\hat{G}(q;\theta)u(t - n_k)$$
$$+ (1 - \hat{H}^{-1}(q;\theta))y(t) \tag{8a}$$

and the quantitative comparison of the result with the experimentally recorded output, which is carried out based on the calculation of an appropriate form of the loss function.

The parameters of the system could be calculated for different values of the model's order (n, in the case of the ARMAX($n,n,n,1$) model structure introduced in Section IV), but the final selection was based on the level of the "fitness" [48] calculated through the following relation:

$$\text{fitness} = 100 \cdot \left(1 - \sqrt{\frac{N \cdot V_N(\hat{\theta})}{\sum_{t=1}^{N}(y(t) - y_m)^2}}\right) \% \tag{9a}$$

in which y_m is the mean value of $y(t)$. The criterion was to select the smallest order which could lead to acceptably high fitness levels in the whole considered range of the experimentally obtained data.

REFERENCES

[1] N. Yamazoe, "Toward innovations of gas sensor technology," *Sens. Actuators B.*, vol. 108, no. 1–2, pp. 2–14, 2005.

[2] N. Barsan, D. Koziej, and U. Weimar, "Metal oxide-based gas sensor research: How to?," *Sens. Actuators B*, vol. 121, no. 1, pp. 18–35, 2007.

[3] S. R. Morrison, "Semiconductor gas sensors," *Sens. Actuators*, vol. 2, pp. 329–341, 1982.

[4] P. T. Moseley, "Solid state gas sensors," *Meas. Sci. Technol.*, vol. 8, no. 3, pp. 223–237, 1997.

[5] S. Akbar, P. Dutta, and C. Lee, "High temperature ceramic gas sensors: A review," *Int. J. Appl. Ceramic Technol.*, vol. 3, no. 4, pp. 302–311, 2006.

[6] W. Gopel and K. D. Schierbaum, "SnO$_2$ sensors: Current status and future prospects," *Sens. Actuators B*, vol. 26, no. 1–3, pp. 1–12, 1995.

[7] G. Korotchenkov, V. Brynzari, and S. Dmitriev, "SnO$_2$ thin film gas sensors for fire-alarm systems," *Sens. Actuators B.*, vol. 54, no. 3, pp. 191–196, 1999.

[8] K. Persaud and G. H. Dodd, "Analysis of discrimination mechanisms in the mammalian olfactory system using a model nose," *Nature*, vol. 299, pp. 352–355, 1982.

[9] H. T. Nagel, R. Gutierrez-Osuna, and S. S. Schiffman, "The how and why of electronic noses," *IEEE Spectrum*, vol. 35, no. 9, pp. 22–31, 1998.

[10] J. W. Gardner and P. N. Bartlett, "A brief history of electronic noses," *Sens. Actuators B.*, vol. 18–19, no. 1–3, pp. 211–220, 1994.

[11] M. A. Craven, J. W. Gardner, and P. N. Bartlett, "Electronic noses-development and future prospects," *Trends Anal. Chem.*, vol. 15, no. 9, 1996.

[12] H. Windischmann and P. Mark, "A model for the operation of a thin-film SnO$_x$ conductance-modulation carbon monoxide sensor," *J. Electrochem. Soc.: Solid-State Science and Technol.*, vol. 126, no. 4, pp. 627–633, 1979.

[13] D. E. Williams, "Conduction and gas response of semiconductor gas sensor," in *Solid State Gas Sensors*, P. T. Moseley and B. C. Tofield, Eds. Bristol, U.K.: Adam Hilger, 1987, ch. 5.

[14] S. R. Morrison, "Mechanism of semiconductor gas sensor operation," *Sens. Actuators*, vol. 11, pp. 283–287, 1987.

[15] A. Fort, S. Rocchi, M. B. Serrano-Santos, R. Spinicci, and V. Vignoli, "Surface state model for conductance responses during thermal-modulation of SnO$_2$-based thick film sensors: Part I, model derivation," *IEEE Trans. Instrum. Meas.*, vol. 55, no. 6, pp. 2102–2106, 2006.

[16] S. R. Morrison, "Selectivity in semiconductor gas sensors," *Sens. Actuators*, vol. 12, no. 4, pp. 425–440, 1987.

[17] F. Hossein-Babaei and M. Orvatinia, "A novel approach to hydrogen sensing," *IEEE Sensors J.*, vol. 4, no. 6, pp. 802–806, 2004.

[18] F. Hossein-Babaei and M. Orvatinia, "Transient regime of gas diffusion-physisorption through a microporous barrier," *IEEE Sensors J.*, vol. 5, no. 5, pp. 1004–1010, 2005.

[19] S. Nicoletti, S. Zampolli, I. Elmi, L. Dori, and M. Severi, "Use of different sensing materials and deposition techniques for thin-film sensors to increase sensitivity and selectivity," *IEEE Sensors J.*, vol. 3, no. 4, pp. 454–459, 2003.

[20] G. Tournier, C. Pijolat, R. Lalauze, and B. Patissier, "Selective detection of CO and CH$_4$ with gas sensors using SnO$_2$ doped with palladium," *Sens. Actuators B*, vol. 26–27, no. 1–3, pp. 24–28, 1995.

[21] R. Muller, E. Schweizer, and E. Lange, "Gas analysis method using response time constant," Canadian Patent CA 1248176, 1989.

[22] A. P. Lee and B. J. Reedy, "Temperature modulation in semiconductor gas sensing," *Sens. Actuators B*, vol. 60, no. 1, pp. 35–42, 1999.

[23] W. M. Sears, K. Colbow, and F. Consadori, "General characteristics of thermally cycled tin oxide gas sensors," *Semicond. Sci. Technol.*, vol. 4, pp. 351–359, 1989.

[24] A. Vergara, E. Llobet, J. Brezmes, X. Vilanova, P. Ivanov, I. Grácia, C. Cané, and X. Correig, "Optimized temperature modulation of micro-hotplate gas sensors through pseudorandom binary sequences," *IEEE Sensors J.*, vol. 5, no. 6, pp. 1369–1378, 2005.

[25] R. Gutierrez-Osuna, A. Gutierrez-Galvez, and N. Powar, "Transient response analysis for temperature-modulated chemoresistors," *Sens. Actuators B*, vol. 93, no. 1–3, pp. 57–66, 2003.

[26] S. Nakata, E. Ozaki, and N. Ojima, "Gas sensing based on the dynamic non-linear responses of a semiconductor gas sensor: Dependence on the range and frequency of a cyclic temperature change," *Anal. Chem. Acta.*, vol. 361, no. 1, pp. 93–100, 1998.

[27] T. A. Kunt, T. J. McAvoy, R. E. Cavicchi, and S. Semancik, "Optimization of temperature programmed sensing for gas identification using micro-hotplate sensors," *Sens. Actuators B*, vol. 53, no. 1–2, pp. 24–43, 1998.

[28] T. Amamoto, T. Yamaguchi, Y. Matsuura, and Y. Kajiyama, "Development of pulse-drive semiconductor gas sensor," *Sens. Actuators B*, vol. 13–14, no. 1–3, pp. 587–588, 1993.

[29] E. L. Hines, E. Llobet, and J. W. Gardner, "Electronic noses: A review of signal processing techniques," *IEE Proc. Circuits, Devices, and Syst.*, vol. 146, no. 6, pp. 297–310, 1999.

[30] S. Marco, A. Pardo, F. A. M. Davide, C. Di Natale, A. D'Amico, A. Hierlemann, J. Mitrovics, M. Schweizer, U. Weimar, and W. Gopel, "Different strategies for the identification of gas sensing systems," *Sens. Actuators B.*, vol. 34, no. 1–3, pp. 213–223, 1996.

[31] A. Pardo, S. Marco, and J. Samitier, "Nonlinear inverse dynamic models of gas sensing based on chemical sensor arrays for quantitative measurements," *IEEE Trans. Instrum. Meas.*, vol. 47, no. 3, pp. 644–651, 1998.

[32] A. Pardo, S. Marco, J. Samitier, F. A. M. Davide, C. Di Natale, and J. Samitier, "Dynamic measurements with chemical sensor arrays based on inverse modeling," in *Proc. IEEE Instrum. Meas. Technol. Conf.*, Brussels, Belgium, 1996, pp. 904–907.

[33] F. Derbel, "Modeling fire detector signals by means of system identification techniques," *IEEE Trans. Instrum. Meas.*, vol. 50, no. 6, pp. 1815–1821, 2001.

[34] G. E. Searle, J. W. Gardner, M. J. Chappell, K. R. Godfrey, and M. J. Chapman, "System identification of electronic nose data from cyanobacteria experiments," *IEEE Sensors J.*, vol. 2, no. 3, pp. 218–229, 2002.

[35] E. Llobet, J. Brezmes, X. Vilanova, L. Fondevila, and X. Correig, "Quantitative vapor analysis using the transient response of non-selective thick film tin oxide gas sensors," in *Proc. IEEE Transducers*, Chicago, USA, 1997, vol. 2, pp. 971–974.

[36] S. A. Billings, "Introduction to non-linear system analysis and identification," in *Signal Processing for Control*, K. Godfrey and P. Jones, Eds. Berlin, Germany: Springer-Verlag, 1985, cited by [31].

[37] K. Fukunaga, *Introduction to Statistical Pattern Recognition*, 2nd ed. San Diego, CA: Academic, 1991, ch. 9.

[38] R. O. Duda, P. E. Hart, and D. G. Stork, *Pattern Classification.*, 2nd ed. New York: Wiley, 2001, ch. 4.

[39] R. Gutierrez-Osuna, "Pattern analysis for machine olfaction: A review," *IEEE Sensors J.*, vol. 2, no. 3, pp. 189–202, 2002.

[40] L. Ljung, *System Identification, Theory for the User*, 2nd ed. Englewood Cliffs, NJ: Prentice-Hall, 1999, ch. 4, 10, 16.

[41] T. Soderstrom and P. Stoica, *System Identification*. London, U.K.: Prentice-Hall Int., 1989, ch. 6 and 7.

[42] G. E. P. Box and G. M. Jenkins, "Time series analysis," in *Forecasting and Control*. San Francisco, CA: Holden-Day, 1970.

[43] O. Nelles, *Nonlinear System Identification*. Berlin, Germany: Springer-Verlag, 2001, ch. 16.

[44] Q. Song, F. Liu, and R. D. Findlay, "Generalized predictive control for a pneumatic system based on an optimized ARMAX model with an artificial neural network," *Proc. CIMCA-IAWTIC'06, IEEE 2006*, pp. 223–223, Nov. 2006.

[45] FIS Inc. [Online]. Available: http://www.fisinc.co.jp/

[46] M. Falasconi, M. Pardo, G. Sberveglieri, I. Riccò, and A. Bresciani, "The novel EOS^{835} electronic nose and data analysis for evaluating coffee ripening," *Sens. Actuators B.*, vol. 110, no. 1, pp. 73–80, 2005.

[47] J. E. Dennis and R. B. Schnabel, *Numerical Methods for Unconstrained Optimization and Nonlinear Equations*. Englewood Cliffs, NJ: Prentice-Hall, 1983, ch. 10.

[48] L. Ljung, *System Identification Toolbox 7 User's Guide*. Natick, MA: MathWorks, Inc., 2007.

Faramarz Hossein-Babaei (M'05) received the B.S. degree in electronic engineering from Amir-Kabir Industrial University, Tehran, Iran, in 1971, and the M.S. degree in materials science and the Ph.D. degree in electrical engineering from Imperial College, London, U.K., in 1975 and 1978, respectively.

He is Professor of Electronic Materials at the Electrical Engineering Department, K. N. Toosi University of Technology, Tehran. He has founded a number of hi-tech spinoff companies mostly active in the field of high-temperature materials and technology. He is also an Adjunct Professor at the Faculty of Applied Science, University of British Columbia, Vancouver, BC, Canada. His present research interests include electric heating, electrophoretic deposition of electroceramic materials, microfluidics, metal-oxide gas sensors, and artificial olfaction.

Prof. Hossein-Babaei is a member of the American Ceramic Society.

Seyed Mohsen Hosseini Golgoo received the B.S. degree from Semnan University, Semnan, Iran, in 2001 and the M.S. degree from K. N. Toosi University of Technology, Tehran, Iran, in 2003, both in electronic engineering. He is currently working towards the Ph.D. degree at the Department of Electrical Engineering, K. N. Toosi University of Technology.

His research interests include machine olfaction, system identification, and sensors fabrication and modeling.